Journal of Materials Chemistry A

Accepted Manuscript

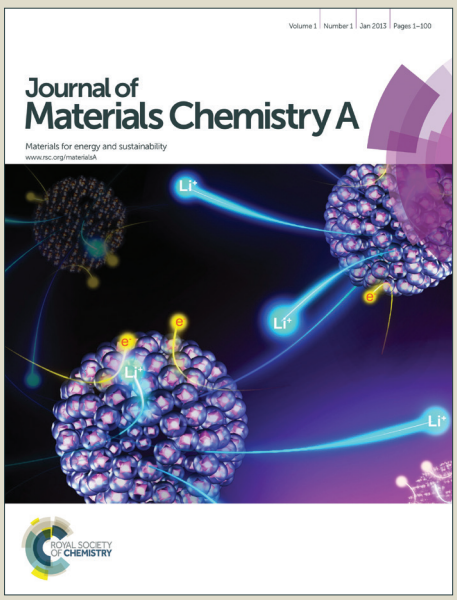

ROYAL SOCIETY OF CHEMISTRY

www.rsc.org/materialsA

Journal Name

RSCPublishing

PAPER

α-Fe_2O_3 spherical nanocrystals supported on CNTs as efficient non-noble electrocatalyst for oxygen reduction reaction

Cite this: DOI: 10.1039/x0xx00000x

Received 00th January 2012,
Accepted 00th January 2012

DOI: 10.1039/x0xx00000x

www.rsc.org/

Meng Sun,[a,c] Youzhen Dong,[b] Gong Zhang,[a,c] Jiuhui Qu,*[a] and Jinghong Li,*[b]

Substitution of low cost and non-noble catalyst for expensive and scarce Pt to optimize oxygen reduction reaction (ORR) aimed to economical application in fuel cells is crucial for solving the world-wide energy crisis in the future. A novel α-Fe_2O_3/CNTs nanocatalyst was synthesized via facile nucleation and crystal growth of α-Fe_2O_3 on carbon nanotubes (CNTs) under annealing process. The characterizations of X-ray diffraction (XRD), transmission electron microscopy (TEM) and X-ray photoelectron spectroscopy (XPS) indicated that spherical α-Fe_2O_3 nanocrystals had good dispersion on the surface of CNTs and were compactly stuck in the spatial structure. The catalytic activity of ORR revealed that the process over α-Fe_2O_3/CNTs was almost twice higher than CNTs and α-Fe_2O_3, respectively. The α-Fe_2O_3 loading on CNTs had great influence on catalytic performance for ORR and the special trigonal structure of α-Fe_2O_3 was beneficial for elevation of ORR electroactivity. The kinetics studies suggested the α-Fe_2O_3/CNTs processed with nearly four-electron-transfer pathway in ORR. Strong methanol tolerance and long durability further promoted the superiority of α-Fe_2O_3/CNTs.

Introduction

The oxygen reduction reaction (ORR) plays a vital role in solving worldwide energy crisis in the near future.[1] Generally, the sluggish kinetic process of ORR contains a desirable four-electron-transfer pathway with the formation of H_2O as end products and an undesirable two-electron-transfer process with the generation of hydrogen peroxide, which has become the key factors limiting its performance in corrosion prevention[2] and energy conversion.[3]

Precious metals platinum (Pt) have aroused great interest in developing noble electrocatalytic materials for ORR study due to the successful application of commercial Pt/C catalysts in fuel cells and metal–air batteries in recent decades. Although the following researches focused on advanced precious metals with specific shapes,[4] bimetallic/intermetallic composition,[5] and core-shell structures[6] have acquired some achievements in optimizing the catalytic activity for ORR, some drawbacks such as high cost, crossover effects and CO poisoning[7] are still intractable. Thus, developing low-cost and efficient catalysts for ORR in order to expand practical application is essential.

Non-noble catalysts such as transition-metal chalcogenides,[8] nitrides,[9-11] oxides[12] and heteroatom-doped carbonaceous (e.g. graphene)[13] have been recently identified for highly catalyzing the ORR. Moreover, in addition to the superiority of economy, other advantages such as the hierarchically porous structures,[14] highly conductive network,[15] and especially the heterogeneous growing or assembling of transition-metal oxides with special nanocrystal structure supported on carbonaceous substrates[16,17] have exhibited remarkable electrocatalytic performance in ORR. Yang et al.[18] prepared MnO_x/carbon nanotubes (0.85 wt % MnO_x) catalyst for ORR, and it had a high ORR activity compared with Pt/C due to the high positive charge generated on the surface of catalyst.

Carbon nanotubes (CNTs), which have sp^2-hybirdized carbon networks, exhibit high surface area, good conductivity, strong mechanical property and stability. Several research groups have reported that CNTs-based electrodes can markedly improve catalytic behavior compared to conventional carbon-contained materials as catalyst supports. As Chen et al.[19] reported, the metal/metal-oxide nanoparticles encapsulated and dispersed in/on the CNTs contribute to the excellent increases of redox behavior of composites. Furthermore, appropriate low-load transition-metal oxides (e.g. MnO_x, FeO_y, and CoO_z)

supported on CNTs avoid their defects on poor electrical conductivity, but distinctly exhibit their electrocatalytic activity due to the activate sites of electron hole caused by their special crystalline structure.[20-23] α-Fe_2O_3 has been studied extensively because of its superior performance as the active electrode materials in pseudocapacitors,[24] lithium batteries[25] and photoelectrochemical oxidation.[26] The reported high catalytic activity of α-Fe_2O_3 is attributed to the active redox behavior of Fe^{3+}/Fe^{2+} cations in its trigonal structure. It is reasonable that the polymorphism and valence states of Fe cations exposed on active crystal faces are beneficial for high-performing for ORR on α-Fe_2O_3 catalysts. Therefore, cooperatively integrating α-Fe_2O_3 with CNTs is promising for synthesizing a highly catalytic, strongly durable and low-cost catalyst for ORR.

Herein, a novel and well-structured nanocomposite of low-loaded α-Fe_2O_3 nanocrystals supported on CNTs was successfully synthesized through a simple and mild methods, including facile grain nucleation, solid-phase crystal growing and successive oxygen/nitrogen annealing. X-ray diffraction (XRD), scanning electron microscopy (SEM), transmission electron microscopy (TEM) and X-ray photoelectron spectroscopy (XPS) were employed to characterize α-Fe_2O_3/CNTs nanocomposites. The results indicated that pure α-Fe_2O_3 nanospheres with perfect crystalline structure were well dispersed on the surface of CNTs, which maximized catalytic characteristics of nanocomposites. Furthermore, α-Fe_2O_3/CNTs nanocomposites exhibited an excellent catalytic performance for ORR within a nearly four-electron pathway. The super methanol tolerance and long-term durability compared with commercial Pt/C catalysts in alkaline media, promoting the promising utilization of α-Fe_2O_3/CNTs in fuel cells.

Experimental

Chemicals

Nafion emulsion (5 wt %, Dupont) was supplied by Alfa Aesar. CNTs were obtained from Tsinghua University (Beijing, China). Ultrapure water was produced by a Millipore Water Purification System (Advantage A10, Millipore) with a resistivity of ≥ 18.2 MΩ·cm. Other chemical reagents were purchased from Sino pharm Chemical Reagent Co., Ltd. (Shanghai, China) and used as received.

Synthesis of the activated CNTs

1 g of pristine CNTs were firstly dispersed in 50 mL concentrated nitric acid (HNO_3, 68 wt %) and refluxed at 110 ^oC in oil bath for 6 h, then cooled down to room temperature. The mixture was filtered through a nylon 66 film (0.2 μm) and washed by ultrapure water for several times until the pH of filtrate reached to 7. After the resulting products were dried at 60 ^oC for 12 h, the activated CNTs were well prepared to further synthesis.

Synthesis of α-Fe_2O_3 and α-Fe_2O_3/CNTs nanocomposites

The α-Fe_2O_3 was produced by hydrolysis of Fe(Ⅲ) salt solutions. Firstly, 1 L of 0.001M HNO_3 was heated in a Duran flask to 95 ^oC in oven. Then, 8.4 g unhydrolyzed $Fe(NO_3)_3·9H_2O$ was rapidly added into the vessel and vigorously stirred after the solution maintained at 95 ^oC for 30 min. The mixture was held in the oven for 48 h at 95 ^oC until the compact, bright red sediment was formed. The sediment was washed by ultrapure water for three times and dried at room temperature. Finally, the resulting products were mildly heated to 140 ^oC in air and kept for 8 h, and then heated to 450 ^oC in nitrogen and held for 3 h.

For preparing the α-Fe_2O_3/CNTs nanocomposites,[19] 100 mg of activated CNTs were stirring at 600 rpm in ethanol/water (v/v = 5%) solution at room temperature for 1 h followed by 10 min ultrasonic treatment. Subsequently, a fresh aqueous $Fe(NO_3)_3$ was added quickly and the solvent was dried at 60 ^oC for 12 h. Finally, the dried composites were mildly heated to 140 ^oC in air, kept for 8 h, and then heated to 450 ^oC in nitrogen and held for 3 h.

Characterizations

Powder X-ray diffraction (XRD) of the catalyst was recorded on a D8 Advance (Bruker) X-ray Diffractometer with Cu Kα radiation (λ = 1.54059 Å). The step size and scan rate were set as 0.05° and 0.025° s^{-1}, respectively. Transmission electron microscopy (TEM) and high resolution transmission electron microscopy (HRTEM) images were obtained with a TEM H-800 (Hitachi, Japan) at an accelerating voltage at 200 kV. The X-ray photoelectron spectroscopy (XPS) data were taken on an AXIS-Ultra instrument (Kratos Analytical, UK) using monochromatic Al Kα radiation (225 W, 15 mA, 15 kV) and low-energy electron flooding for charge compensation. Binding energies were calibrated using the C1s hydrocarbon peak at 284.80 eV in order to compensate for surface charge effects.

Electrochemical experiments

The electrochemical cell was assembled with a conventional three-electrode system: a working glassy carbon electrode (GCE), an Ag|AgCl/KCl (saturated) reference electrode and Pt wire as a counter electrode. The surface of GCE was firstly polished by using 0.3 μm Al_2O_3 slurry and washed with ethanol and ultrapure water in ultrasonic bath before used. Then the clean GCE should cycle at 50 mV s^{-1} between 0 and -0.7 V until reproducible cyclic voltammograms were obtained. Catalyst ink was obtained by mixing sold catalyst (1 mg) with Nafion solution (1 mL, 0.5 wt %, aq) under 30 min sonication for total dispersing. Finally, 6 and 20 μL of the catalyst inks were dropped onto the prepared GCE with diameter of 3 and 5 mm, respectively. Electrochemical measurements were performed by using a CHI 830 electrochemical analyzer coupled with a rotating-disk electrode (RDE) system (Princeton Applied Research, Model 616). All experiments were operated at room temperature.

Results and discussion

Fig. 1A shows the powder X-ray diffraction patterns of CNTs, α-Fe_2O_3 and α-Fe_2O_3/CNTs nanocomposites, respectively. Several strong diffraction peaks can be observed corresponding to (012), (104), (110), (113), (024), (116), (214) and (300) peaks from α-Fe_2O_3/CNTs, which are precisely matched with pure α-Fe_2O_3 crystal (JCPDS No. 33-0664). Through the facile synthetic process, the α-Fe_2O_3/CNTs nanocomposites did not exhibit characteristic peaks corresponding to the CNTs, which suggested that better crystalline α-Fe_2O_3 nanocrystals successfully supported on CNTs, and resulted in no distinct carbon peak.

Typical scanning electron microscopy (SEM), transmission electron microscopy (TEM) and high resolution transmission

electron microscopy (HRTEM) images provide insight into the morphologies and structures of α-Fe_2O_3/CNTs (Fig. SI-1). Fig. 1B reveals that spherical α-Fe_2O_3 nanocrystals with an approximate diameter of 20 nm are scattered on CNTs. Remarkably, α-Fe_2O_3 nanocrystals are stably stuck in the compact three-dimensional spatial structure formed by the stacked nanotubes. The spatial structure built by CNTs may determine the diameter of α-Fe_2O_3 nanocrystals to some extent. The corresponding HRTEM image (insets of Fig. 1B) demonstrates that a well-defined crystalline lattice can be observed with a lattice spacing of 0.264 nm, corresponding to the (104) plane of α-Fe_2O_3 nanocrystal.

The α-Fe_2O_3/CNTs nanocomposites were further characterized by the X-ray photoelectron spectroscopy to confirm the elementary composition and metallic state of Fe. As shown in Fig. 1C, only C 1s, O1s and Fe 2p can be found with their corresponding binding energies (BE) without any impurity. High resolution XPS spectra of C 1s, O 1s and Fe 2p of the α-Fe_2O_3/CNTs nanocomposites are shown in Fig. 1D. The XPS spectrum of C 1s is preferably corresponded with the following carbon bonding: 284.6 eV (C–C), 288.6 eV (C–O–C and C–O–H). Similarly, the peaks at 529.9, 531.5 and 533.4 eV of the O 1s spectrum are mainly fitted to the signal of the ferric oxides (Fe_2O_3), oxygen bridge (–O–) on the interfaces of the structure and the residual –OH and –COOH groups on CNTs, respectively. The peaks at 711 eV, 719 eV and 724 eV represent the binding energies of Fe $2p_{3/2}$, shake-up satellite Fe $2p_{3/2}$, and Fe $2p_{1/2}$ of Fe^{3+}. Moreover, no obvious signals are detected for Fe^0 at 707 eV and Fe $2p_{3/2}$ of Fe^{2+} at 709.5 eV, suggesting the excellent formation of pure ferric oxides without impurities.

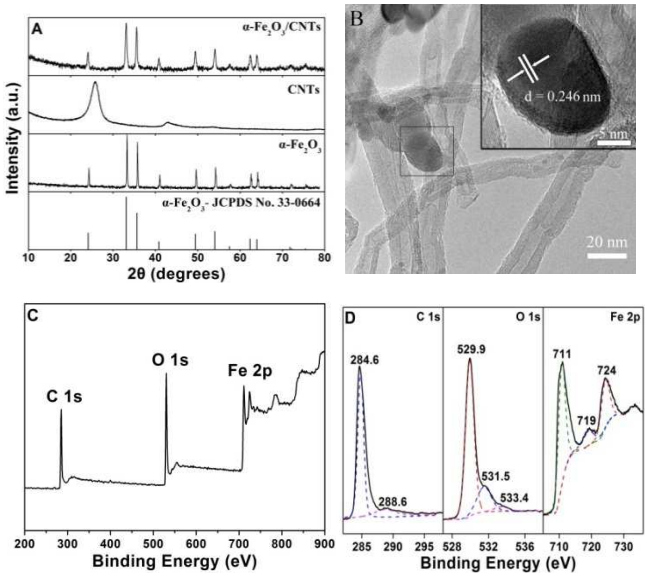

Fig.1 (A) XRD patterns of CNTs, α-Fe_2O_3 and α-Fe_2O_3/CNTs nanocomposites. (B) TEM image of α-Fe_2O_3/CNTs. The Inset shows the corresponding HRTEM image of α-Fe_2O_3 nanocrystals on CNTs. (C) XPS spectra of α-Fe_2O_3/CNTs nanocomposites. (D) High resolution XPS spectra of C 1s, O 1s and Fe 2p of α-Fe_2O_3/CNTs nanocomposites.

Fig. 2A shows the cyclic voltammograms (CVs) of ORR in N_2 and O_2-saturated 0.1 M KOH solution of CNTs, α-Fe_2O_3 and α-Fe_2O_3/CNTs nanocomposites, respectively. Indistinctive redox peak of α-Fe_2O_3/CNTs nanocomposites was observed in N_2-saturated solution (dashed line in Fig. 2A) in the potential range from 0 to -0.7 V. However, distinct peaks corresponding to the ORR could be found for all electrode materials in the oxygen-enriched solution, which verified the obvious electrocatalytic activity for ORR. The limiting current density of α-Fe_2O_3/CNTs for ORR electrocatalysis was two times higher than α-Fe_2O_3 and CNTs, respectively. Fig. 2A illustrates that a steep increase in the reduction peak current density was observed with 1.31 mA cm^{-2} at peak potential of -0.27 V for α-Fe_2O_3/CNTs, but only 0.52 mA cm^{-2} at -0.38 V for α-Fe_2O_3, 0.53 mA cm^{-2} at -0.54 V for CNTs. Correspondingly, the onset and peak potentials of α-Fe_2O_3/CNTs were decreased about 0.1 and 0.11 V towards α-Fe_2O_3, 0.24 and 0.27 V towards CNTs, respectively. It demonstrates that α-Fe_2O_3/CNTs have pronounced catalytic performance compared with α-Fe_2O_3 and CNTs. This CV curve of α-Fe_2O_3/CNTs also possessed excellent behaviors, as compared to that of Fe_x-CNTs reported elsewhere.[27,28]

Additionally, different mole ratios of Fe and C from 1:10000 to 1:1 were evaluated to investigate the effect of Fe-loading on electrocatalytic activity (Fig. SI-2). The results indicated that the optimum mole ratio of Fe and C was 1:100, resulting in the biggest limiting current density and lowest onset and peak potentials. Such appropriate loading of α-Fe_2O_3 supported on CNTs is beneficial to ORR due to the advantages of appropriate loading and optimised nano-construction of nanocomposites. Furthermore, this architectural feature of catalyst is apt to act as an accelerator of charge transfer on the surface of material, which can reduce resistance and increase stability of the transportation between free electrons and oxygen.[29,30]

Linear sweep voltammetry (LSV) curves were measured by rotating-disk electrode (RDE) in O_2-saturated 0.1 M KOH solution at a rotation rate of 1600 rpm to investigate the electrocatalytic performance of the above catalysts during the ORR process. In Fig. 2B, α-Fe_2O_3/CNTs had a more positive onset potential (-0.15 V) and higher limiting current density (3.89 mA cm^{-2}) at -0.6 V than α-Fe_2O_3 (-0.18 V and 2.77 mA cm^{-2}) and CNTs (-0.22 V and 2.33 mA cm^{-2}), only a little weaker than that of Pt/C (-0.1 V and 4.03 mA cm^{-2}) at the same rotation rate (Fig. SI-3A). These results are agreed with those obtained from CV measurement, and further confirm that α-Fe_2O_3/CNTs had superior catalytic activity in ORR owing to its special structural characteristics of appropriate α-Fe_2O_3 decorated on CNTs, which possessed more activity sites, improved electrolyte diffusion and faster interfacial charge transfer.

The electron transfer number (n) involved in the oxygen reduction at each electrode was analyzed by RDE and calculated on the basis of the Koutecky-Levich (K-L) equations given below [Eqs. (1)-(3)]:[31]

$$\frac{1}{J}=\frac{1}{J_K}+\frac{1}{J_L}=\frac{1}{B\omega^{\frac{1}{2}}}+\frac{1}{J_K} \quad (1)$$

$$B=0.62nFC_0D_0^{\frac{2}{3}}v^{-\frac{1}{6}} \quad (2)$$

$$J_K=nFkC_0 \quad (3)$$

where J is the measured current density, J_K and J_L are the kinetic and diffusion limiting current densities, ω is the electrode rotating rate ($\omega=2\pi N$, N is the linear rotation speed), n is the overall number of electrons transferred in the oxygen reduction, F is the Faraday constant (96485 C mol^{-1}), C_0 is the bulk concentration of O_2, D_0 is the diffusion coefficient of O_2 in

the KOH electrolyte, v is the kinematic viscosity of the electrolyte, and k is the electron transfer rate constant.

The corresponding K-L plots[32] have good linearity with parallelism, suggesting a similar electron-transfer number per O_2 molecule involved and first-order dependence of O_2 kinetics in the ORR. As can be seen from Fig. 2C, different materials have good linearity. According to Equations (1) and (2), n was calculated to be 3.05 at -0.60 V for CNTs, 3.12 at -0.60 V for α-Fe_2O_3 and 3.45 at -0.60 V for α-Fe_2O_3/CNTs, respectively. This result indicated that the CNTs and α-Fe_2O_3 both processed in combined two-electron and four-electron pathways, but α-Fe_2O_3/CNTs was in a nearly four-electron pathway. Based on the Equations (3), the calculated kinetics current densities for CNTs, α-Fe_2O_3 and α-Fe_2O_3/CNTs are 6.19, 7.39 and 18.48 mA cm^{-2} at -0.60 V, further indicating a notable ORR activity of α-Fe_2O_3/CNTs catalyst.

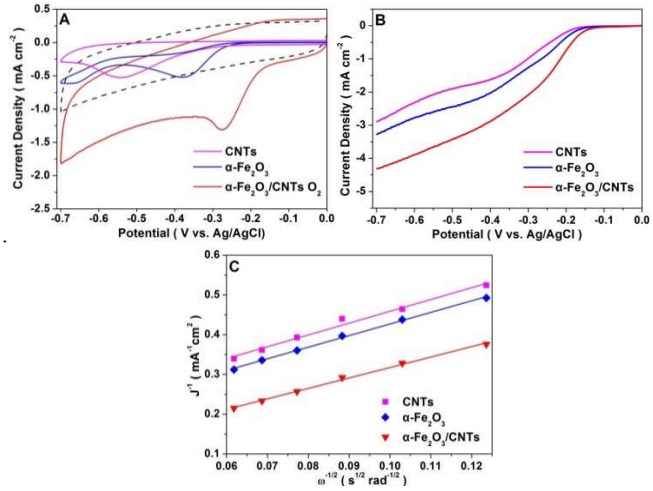

Fig.2 (A) CV curves of CNTs, α-Fe_2O_3 and α-Fe_2O_3/CNTs nanocomposites at a scan rate of 50 mV s^{-1} in O_2 (solid line) and N_2 (dashed line of α-Fe_2O_3/CNTs) -saturated 0.1 M KOH. (B) LSV curves of CNTs, α-Fe_2O_3 and α-Fe_2O_3/CNTs nanocomposites in O_2-saturated 0.1 M KOH solution at a rotation rate of 1600 rpm. Sweep rate: 5 mV s^{-1}. (C) The corresponding Koutecky–Levich plots of CNTs, α-Fe_2O_3 and α-Fe_2O_3/CNTs nanocomposites at -0.6 V.

Further insight was gained into the ORR activity of the α-Fe_2O_3/CNTs nanocomposites through RDE voltammetry in order to study the kinetics of the electrochemical catalytic. The polarization curves were obtained by scanning the potential from 0 to -0.7 V at a scan rate of 5 mV s^{-1} with various rotation rates in O_2-saturated 0.1 M KOH solution. In Fig. 3A, the higher limiting current density can be observed with increasing rotation rate. In addition, different α-Fe_2O_3/CNTs with the mole ratios of Fe and C from 1:1 to 1:125 in O_2-saturated 0.1 M KOH solution at various rotation rates also had the similar trends (Fig. SI-3). The average calculated n was 3.56 and J_K was 16.46 mA cm^{-2} at the potential from -0.45 to -0.65 V for α-Fe_2O_3/CNTs nanocomposites (Fig. 3B). This result demonstrates that the α-Fe_2O_3/CNTs nanocatalysts preferred involving in a nearly four-electron transfer process that reduces O_2 directly to OH^- in ORR close to commercial Pt/C (n=3.89).[33]

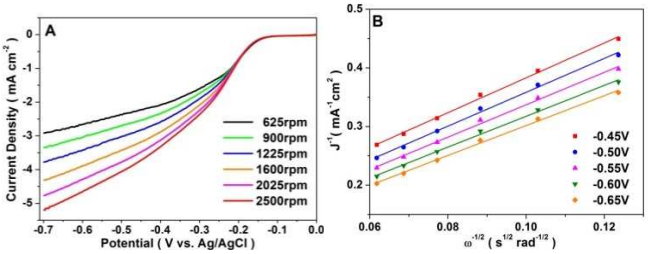

Fig.3 (A) RDE curves of α-Fe_2O_3/CNTs nanocomposites with mole ratio of Fe and C 1:100 in O_2-saturated 0.1 M KOH solution at various rotation rates. Sweep rate: 5 mV s^{-1}. (B) The corresponding Koutecky–Levich plots of α-Fe_2O_3/CNTs nanocomposites at different potentials derived from the RDE measurements.

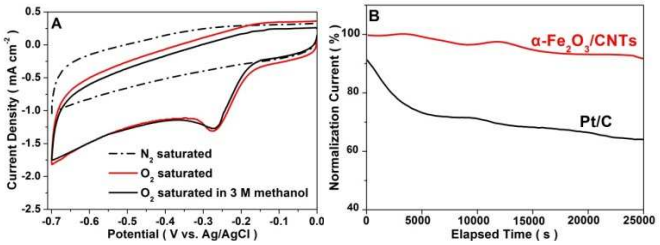

Fig.4 (A) CV curves of α-Fe_2O_3/CNTs nanocomposites with mole ratio of Fe and C 1:100 in N_2 and O_2-saturated 0.1 M KOH solutions as well as O_2-saturated 0.1 M KOH solution with 3 M methanol. Scan rate: 50 mV s^{-1}. (B) Current–time (I–t) responses of α-Fe_2O_3/CNTs nanocomposites and Pt/C at -0.30 V in O_2-saturated 0.1 M KOH solutions. The rotation rate is 1600 rpm.

Strong methanol tolerance is essential for new ORR catalysts in fuel cells, and the crossover effects were assessed on CNTs, α-Fe_2O_3, α-Fe_2O_3/CNTs nanocomposites and commercial Pt/C (Fig. 4A and Fig. SI-4). The α-Fe_2O_3/CNTs performed excellently compared to Pt/C. A similar catalytic activity for α-Fe_2O_3/CNTs was observed after adding 3 M methanol into an O_2-saturated 0.1 M KOH solution. In contrast, nearly no peak could be found for Pt/C, indicating no methanol tolerance and was even worse than those of CNTs and α-Fe_2O_3 (Fig. SI-4). The durability of the α-Fe_2O_3/CNTs nanocomposites and Pt/C catalyst for ORR was evaluated by chronoamperometry at -0.3 V in O_2-saturated 0.1 M KOH solutions at a rotation rate of 1600 rpm. It can be seen from Fig. 4B that after continuous reaction for 25000 s, the current density loss on α-Fe_2O_3/CNTs electrode (9.1%) was much less than that of Pt/C (36%). These results demonstrate that such novel α-Fe_2O_3/CNTs nanocomposites could be used as ideal catalyst for direct methanol fuel cells.

The main reasons of excellent electroactivity of α-Fe_2O_3/CNTs nanocomposites preforming in ORR can be summarized as followed. (1) The short hole diffusion length (~2-4 nm), low electron mobility (~10^{-1} cm^2 $V^{-1}s^{-1}$) and efficient charge carrier recombination characteristics of nanocrystal α-Fe_2O_3, yielding promising reductive performance of O_2. (2) Owing to one dimensional structure of CNTs, it has a superior charge transfer rate, improved mass transport and O_2 diffusion.[27] (3) Such appropriate loading of trigonal α-Fe_2O_3 nanocrystals supported on CNTs used as a superstructure can greatly enhance the electrical conductivity and corrosion resistance. (4) Good structural stability and acid/alkali tolerance of CNTs are qualified for being used as substrates, and chemical compatibility with methanol of α-Fe_2O_3 nanocrystals also contributed to the super performance in methanol tolerance and durability.

Conclusions

The α-Fe_2O_3 spherical nanocrystals supported on CNTs were synthesized via mild grain nucleation of $Fe(NO_3)_3$ and solid-phase crystal growth of α-Fe_2O_3 nanocrystals dispersed on CNTs under oxygen and nitrogen annealing, respectively. The characterizations of XRD, TEM and XPS reveal that elliptical sphere of α-Fe_2O_3 nanocrystals with a diameter of 20 nm adhered stably to the surface of CNTs without any impurity. High efficient electrocatalytic ORR activity of α-Fe_2O_3/CNTs nanocomposites was initially obtained from CV measurements, in which the nanocatalysts exhibited high-performing of ORR compared with CNTs, α-Fe_2O_3 and Pt/C due to the peak current density of 1.31 mA cm^{-2} at -0.27 V. The calculated electron transfer number in ORR was 3.56, indicating the kinetics of the electrocatalysis preferred involving in a nearly four-electron transfer process. The α-Fe_2O_3/CNTs nanocomposites had strong methanol tolerance and predominant long durability with only 9.1 % loss on the current density after 25000s. The synthesized α-Fe_2O_3/CNTs nanocomposites with enhanced structural characteristic by low loading of trigonal α-Fe_2O_3 can be obtained as effective non-noble electrocatalyst for the ORR.

Acknowledgements

The work was financially supported by the Major Program of National Natural Science Foundation of China (No. 51290282, No. 21327806), National Basic Research Program of China (No. 2011CB935704, No. 2013CB934004), Research Fund of Ministry of Education of China (No. 20110002130007).

Notes and references

[a] Key Laboratory of Aquatic Science and Technology, Research Center for Eco-Environmental Sciences, Chinese Academy of Sciences, Beijing 100085, China. E-mail: jhqu@rcees.ac.cn
[b] Department of Chemistry, Beijing Key Laboratory for Microanalytical Methods and Instrumentation, Tsinghua University, Beijing 100084, China. E-mail: jhli@mail.tsinghua.edu.cn
[c] University of Chinese Academy of Sciences, Beijing 100039, China

† Electronic Supplementary Information (ESI) available: a series of cyclic voltammograms of Pt/C, α-Fe_2O_3 and α-Fe_2O_3/CNTs in O_2-saturated 0.1 M KOH solutions, and as well as O_2-saturated 0.1 M KOH solution with 3 M methanol, rotating disk voltammograms of Pt/C and α-Fe_2O_3/CNTs in O_2-saturated 0.1 M KOH solutions. See DOI: 10.1039/b000000x/

1. D. W. Wang and D. Su, *Energy Environ. Sci.,* 2014, 7, 576–591.
2. S. G. Chen, Z. d. Wei, X. Q. Qi, L. C. Dong, Y. G. Guo, L. J. Wan, Z. G. Shao and L. Li, *J. Am. Chem. Soc.*, 2012, 134, 13252–13255.
3. B. C. H. Steele and A. Heinzel, *Nature*, 2001, 414, 345–352.
4. A. Kloke, F. von Stetten, R. Zengerle and S. Kerzenmacher, *Adv. Mater.*, 2011, 23, 4976–5008.
5. V. R. Stamenkovic, B. S. Mun, M. Arenz, K. J. J. Mayrhofer, C. A. Lucas, G. Wang, P. N. Ross and N. M. Markovic, *Nat. Mater.*, 2007, 6, 241–247.
6. X. M. Wang, Y. Orikasa, Y. Takesue, H. Inoue, M. Nakamura, T. Minato, N. Hoshi and Y. Uchimoto, *J. Am. Chem. Soc.*, 2013, 135, 5938–5941.
7. V. Komanicky, A. Menzel and H. You, *J. Phys. Chem. B*, 2005, 109, 23550–23557.
8. N. Mahmood, C. Z. Zhang, J. Jiang, F. Liu and Y. L. Hou, *Chem.Eur. J.*, 2013, 19, 5183–5190.
9. M. J. Liu, Y. Z. Dong, Y. M. Wu, H. B. Feng and J. H. Li, *Chem. Eur. J.*, 2013, 19, 14781–14786.
10. L. Wang, J. Yin, L. Zhao, C. G. Tian, P. Yu, J. Q. Wang and H. G. Fu, *Chem. Commun.*, 2013, 49, 3022–3024.
11. J. Yin, L. Wang, C. G. Tian, T. X. Tan, G. Mu, L. Zhao and H. G. Fu, *Chem. Eur. J.*, 2013, 19, 13979–13986.
12. F. Y. Cheng, Y. Su, J. Liang, Z. L. Tao and J. Chen, *Chem. Mater.*, 2010, 22, 898–905.
13. Y. Y. Liang, H. L. Wang, P. Diao, W. Chang, G. Hong, Y. G. Li, M. Gong, L. M. Xie, J. G. Zhou, J. Wang, T. Z. Regier, F. Wei and H. J. Dai, *J. Am. Chem. Soc.*, 2012, 134, 15849–15857.
14. C. X. Xu, Y. Zhang, L. Q. Wang, L. Q. Xu, X. F. Bian, H. Y. Ma and Y. Ding, *Chem. Mat.*, 2009, 21, 3110–3116.
15. Y. Y. Jiang, Y. Z. Lu, X. Y. Lv, D. X. Han, Q. X. Zhang, L. Niu and W. Chen, *ACS Catal.*, 2013, 3, 1263–1271.
16. J. M. Ziegelbauer, T. S. Olson, S. Pylypenko, F. Alamgir, C. Jaye, P. Atanassov and S. Mukerjee, *J. Phys. Chem. C*, 2008, 112, 8839–8849.
17. G. Q. Zhang, S. Wang and F. L. Yang, *J. Phys. Chem. C*, 2012, 116, 3623–3634.
18. Z. Yang, X. M. Zhou, H. G. Nie, Z. Yao and S. M. Huang, *ACS Appl. Mater. Inter.*, 2011, 3, 2601–2606.
19. W. Chen, X. L. Pan and X. H. Bao, *J. Am. Chem. Soc.*, 2007, 129, 7421–7426.
20. D. Eder, *Chem. Rev.*, 2010, 110, 1348–1385.
21. D. H. Deng, L. Yu, X. Q. Chen, G. X. Wang, L. Jin, X. L. Pan, J. Deng, G. Q. Sun and X. H. Bao, *Angew. Chem. Int. Ed.*, 2013, 52, 371–375.
22. Z. Yang, X. M. Zhou, H. G. Nie, Z. Yao and S. M. Huang, *ACS Appl. Mater. Inter.*, 2011, 3, 2601–2606.
23. Z. Yang, X. M. Zhou, Z. P. Jin, Z. Liu, H. G. Nie, X. A. Chen and S. M. Huang, *Adv. Mater.*, 2014, 26, 3156–3161.
24. J. B. Lian, X. C. Duan, J. M. Ma, P. Peng, T. Kim and W. J. Zheng, *ACS Nano*, 2009, 3, 3749–3761.
25. L. W. Ji, O. Toprakci, M. Alcoutlabi, Y. F. Yao, Y. Li, S. Zhang, B. K. Guo, Z. Lin and X. W. Zhang, *ACS Appl. Mater. Inter.*, 2012, 4, 2672–2679.
26. D. K. Zhong, J. W. Sun, H. Inumaru and D. R. Gamelin, *J. Am. Chem. Soc.,* 2009, 131, 6086–6087.
27. B. Ha, O. H. Han, K. J. Hwang, S. Kim and C. K. Rhee, *Electrochim. Acta*, 2011, 58, 422–426.
28. F. J. Pérez-Alonso, M. A. Salam, T. Herranz, J. L. Gómez de la Fuente, S. A. Al-Thabaiti, S. N. Basahel, M. A. Peña, J. L. G. Fierro and S. Rojas, *J. Power Sources*, 2013, 240, 494–502.
29. X. G. Wang, W. Weiss, S. K. Shaikhutdinov, M. Ritter, M. Petersen, F. Wagner, R. Schlögl and M. Scheffler, *Phys. Rev. Lett.*, 1998, 81, 1038–1041.
30. A. Breeuwsma and J. Lyklema, *Discuss. Faraday Soc.*, 1971, 52, 324–333.
31. W. Chen and S. W. Chen, *Angew. Chem.*, 2009, 121, 4450–4453.

32. H. X. Li, Z. F. Bian, J. Zhu, D. Q. Zhang, G. S. Li, Y. N. Huo, H. Li and Y. F. Lu, *J. Am. Chem. Soc.*, 2007, 129, 8406–8407.
33. Y. Z. Dong, Y. M. Wu, M. J. Liu and J. H. Li, *ChemSusChem*, 2013, 6, 2016–2021.